INTERNATIONAL JOURNAL OF NUMERICAL MODELLING: ELECTRONIC NETWORKS, DEVICES AND FIELDS
Int. J. Numer. Model. (2016)
Published online in Wiley Online Library (wileyonlinelibrary.com). DOI:

Using a Jiles-Atherton vector hysteresis model for isotropic magnetic materials with the FEM, Newton-Raphson method and relaxation procedure

Christophe Guérin[1,a,*], Kévin Jacques[2,3] , Ruth V. Sabariego[4], Patrick Dular[3], Christophe Geuzaine[3] and Johan Gyselinck[2]

[1] *CEDRAT, 15 Chemin de Malacher, 38240 Meylan, France*
[2] *Université Libre de Bruxelles, BEAMS department, Brussels, Belgium*
[3] *University of Liège, Department of Electrical Engineering, Institut Montefiore, Liège, Belgium*
[4] *Department of Electrical Engineering (ESAT), EnergyVille, KU Leuven, Leuven, Belgium*

SUMMARY

This paper deals with the use of a Jiles-Atherton vector hysteresis model included in 2D finite element modelling. The hysteresis model is only valid for isotropic materials. It is implemented with the vector potential formulation in 2D along with electric circuit equations to account for a possible external circuit. The Newton-Raphson algorithm is used with a relaxation procedure, whereby at each iteration, the relaxation coefficient is sought so as to minimize the Euclidean norm of the residual of the finite element nonlinear system of equations. We have simulated several numerical examples with the proposed approach. First, simulations on a square domain were carried out so as to validate the model. We have further simulated a T-shaped magnetic circuit (exhibiting rotating flux) and a three-phase three-limb transformer model. For these two cases, the eddy current losses in the laminations are taken into account by a low-frequency model. We have finally performed simulations on the TEAM workshop problem 32 which consists of a three-limb transformer with two windings, for which current and local magnetic flux density measurements are available. We obtained a good agreement between computed and measured results.

KEY WORDS: Finite element method; magnetic hysteresis; Newton-Raphson method; relaxation factor; three-limb transformer

1. INTRODUCTION

In this paper, the 2D magnetic vector potential formulation is used with the finite element (FE) method, the Newton-Raphson (NR) method and the implicit Euler scheme for time stepping. Loss computation accounting for magnetic hysteresis and eddy currents in the lamination stacks of electrical devices, such as transformers and rotating machines, is often performed with a posteriori loss models, i.e. after the resolution. However, when accurate power balance and/or global electrical quantities are sought, e.g.0 when a circuit coupling exists, this a posteriori approach may not be sufficient anymore and the hysteresis model must be included directly in the FE equations.

Such hysteresis models can be either scalar or vectorial [1]. A scalar hysteresis model has a scalar input u(t) and a scalar output f(t). For magnetic materials, a scalar hysteresis model would compute for instance the x-component of the flux density **b** as a function of the x-

[a] Correspondence to: Christophe Guerin, CEDRAT, 15 Chemin de Malacher, Inovallée, 38 246 Meylan Cedex, France.
[*] E-mail: Christophe.Guerin@cedrat.com

component of the magnetic field **h**. A vector hysteresis model is a model which has a vector input **u**(t) and a vector output **f**(t), for instance **h**(t) and **b**(t) respectively. A scalar hysteresis model is not directly usable for a FE simulation of electric devices such as transformers, actuators or rotating machines as the magnetic field has an a priori unknown direction. More importantly, in some areas of the magnetic circuit of these devices, such as in T-joints of transformers or in the stator yoke of rotating machines, the field is rotating. Therefore a vector hysteresis model is needed. Such vector models apply to either anisotropic magnetic materials or only isotropic ones. According to the FE formulation used for the governing magnetic equations, the hysteresis model is either direct, when the magnetic field **h** is the input variable, or inverse, when the flux density **b** is the input variable.

The Jiles-Atherton (JA) hysteresis model [2] is widely employed, because of its small number of parameters, its relative ease of implementation in FE software and its low computational cost compared to other models such as Preisach's [1] [3-5]. Multiple variants of the JA hysteresis model have been proposed, e.g. in [2] [6-16]. A scalar inverse JA model is described in [6]. The vector extension of the scalar direct JA model has first been proposed in [7] for anisotropic materials. Then, the authors of [8] [9] proposed an inverse vector model, based on [6] [7]. A direct vector model has subsequently been developed and used in 3D simulations in [10-12]. Reference [9] deals with the inrush currents of a transformer using the JA inverse vector hysteresis model of [8] with anisotropic materials in its core, so the remanence is taken into account in this part. A direct and inverse JA vector hysteresis model implemented with the NR method and valid only for isotropic magnetic materials is proposed in [13] [14].

Alternatives to the Preisach and JA hysteresis models which are well-suited for FE implementation have also been proposed in the literature. A model based on a chemical reaction analogy is presented in [17] and can be direct or inverse, scalar or vector, and usable for anisotropic materials. An intrinsically vector model is proposed in [18] for isotropic magnetic materials and relies on a consistent thermodynamic formulation. The original model is direct; its inversion is developed in [18]. Other intrinsically vector models are based on vector play operators for isotropic magnetic materials [19] [20]. Models from [18-20] have mathematical similarities with those used in mechanics, in particular for kinematic hardening plasticity.

Note that the identification of the hysteresis models is widely discussed in the literature e.g. in [21] [22] for JA parameters or in [23] for identification of the Bouc–Wen hysteresis model. The methods for the identification of the JA parameters are not discussed in the following of this paper.

In the present paper, we consider the vectorized JA model proposed in [13] [14] together with a 2D magnetic vector potential (MVP) formulation, which requires the inversion of the hysteresis model.

In the case of non-linear non-hysteretic materials, the choice of the NR method is obvious, as it offers a quadratic convergence rate near the solution. However, in the presence of hysteretic materials, the use of the NR is somewhat less evident because convergence is less often reached. The fixed-point method is often used with a hysteresis material, where the convergence is ensured in most cases but is linear [15]. The authors of [6] [8-12] [16] use the differential permeability technique instead of the NR one to solve the FE nonlinear system of equations. However, they report in [11] [12] stability and convergence problems with the direct JA vector hysteresis model and propose some procedures to overcome them: restarting at several previous time steps and time step reduction. In this paper, we explore to use NR

method, because of its quadratic convergence and because we have experience with it in our respective FE software. To our knowledge, a vector JA hysteresis model implemented with the NR method is only proposed in [13] [14]. The novelty of the present paper consists in using the hysteresis model of [13] [14] with an algorithm to determine the relaxation factor at each iteration of the NR algorithm presented in [24], to ensure the NR convergence in most cases.

The paper is organized as follows. First, the numerical aspects of the method are recalled. Then, the method is applied to the simulation of several numerical examples: one relative to a three-phase transformer taking into account the eddy current losses in the laminations with a low-frequency model and a three-limb transformer with two windings for which experimental data (currents and local magnetic flux density measurements) is available.

2. NUMERICAL METHOD

2.1. Magnetic vector potential formulation

We consider a simply-connected domain Ω in the xOy plane. We use the 2D MVP formulation. The magnetic vector potential **a** has only one non-zero z-component orthogonal to the xOy plane defined by:

$$\mathbf{b} = \mathbf{curl}\,\mathbf{a}\,, \tag{1}$$

where **b** is the magnetic flux density. Applying Green's formulas to Ampère's law **curl h** = **j,** where **h** is the magnetic field and **j** the current density, and considering the boundary conditions, the weak form of the MVP formulation is obtained:

$$\int_\Omega \mathbf{curl}\,\mathbf{W}\cdot\mathbf{h}\,\mathrm{d}\Omega = \int_\Omega \mathbf{W}\cdot\mathbf{j}\,\mathrm{d}\Omega\,, \tag{2}$$

where **W** is a test function associated with **a**. Faraday's law $\mathbf{curl}\,\mathbf{e} = -\mathrm{d}\mathbf{b}/\mathrm{d}t$ allows to write the electric field **e** as follows:

$$\mathbf{e} = -\frac{\mathrm{d}\mathbf{a}}{\mathrm{d}t} - \mathbf{grad}\,\mathrm{V}\,, \tag{3}$$

where V is the electric scalar potential. In 2D, the xOy plane is an equipotential of V in each conductor section. The constitutive material laws are accounted for:

$$\mathbf{b} = \mathbf{b}(\mathbf{h}) \text{ or } \mathbf{h} = \mathbf{h}(\mathbf{b}) \text{ and } \mathbf{j} = \sigma\mathbf{e}, \tag{4}$$

where σ is the conductivity (which is supposed scalar and constant).

The domain Ω is discretized with nodal finite elements. The magnetic vector potential is expanded in terms of the vector shape functions $\mathbf{W}_i$, i.e. $\mathbf{W}_i=(0,0,w_i)^t$ with w_i the scalar shape functions and a_i the associated values at the n_p nodes:

DOI:

$$\mathbf{a} = \sum_{i=1}^{n_p} \mathbf{W}_i \, a_i \, . \tag{5}$$

The residuals R_i are obtained from equation (2) taking into account the shape functions $\mathbf{W}_i$. The non-linear system of equations to solve consists of the n_p residuals R_i set to zero:

$$R_i = \int_\Omega \left(\mathbf{curl}\, \mathbf{W}_i \cdot \mathbf{h} - \mathbf{W}_i \cdot \mathbf{j} \right) d\Omega, 1 \le i \le n_p \tag{6a}$$

$$R_i = 0. \tag{6b}$$

The coupling with an external circuit is described in [25]. Herein the additional unknowns are the integrated-in-time electric potentials ψ at nodes of the circuit and the currents in the coils:

$$\psi(t) = \int_{t'=0}^{t} V(t')\, dt', \tag{7}$$

where V is the electric potential.

The coils and the solid conductors are taken into account with the other components of the circuit, by adding circuit equations to the magnetic system of equations (6b). To impose a zero net current in a solid conductor, a circuit equation is added to system (6b) which corresponds to the solid conductor fed by a current source with a zero imposed current:

$$\int_{\Gamma_c} \mathbf{j} \cdot \mathbf{n} \, d\Gamma_c = I = 0 \, , \tag{8}$$

where $\mathbf{n}$ is the normalized Oz-direction vector, and Γ_c the section of the solid conductor.

2.2. Jiles-Atherton vector hysteresis model

We recall in this part the JA inverse vector hysteresis model described in [13] [14]. This model corresponds to the vector extension of the scalar one presented in [7] but limited to the isotropic case. The model is a true vector one, because it computes the magnetic field $\mathbf{h}(t)$, i.e. the three components of $\mathbf{h}(t)$, function of the magnetic flux density $\mathbf{b}(t)$, i.e. the three components of $\mathbf{b}(t)$. Some vector JA hysteresis models have been proposed for instance by [7] [8] [10-12] for anisotropic materials. These models need 5 parameters for each direction (x, y, and z) of the Euclidean space, with a total of 15 parameters. The model proposed by [13] [14] and recalled in this paper is a model only for isotropic materials, with the same five parameter values for the x-, y-, and z-directions. These five parameters are commonly denoted by m_s, a, k, c and α_j, see e.g. [2].

The total magnetization $\mathbf{m}$ consists of a reversible part $\mathbf{m}_{rev}$ added to an irreversible part $\mathbf{m}_{irr}$:

$$\mathbf{m} = \mathbf{m}_{rev} + \mathbf{m}_{irr} \, . \tag{9}$$

An effective field $\mathbf{h}_e$ is defined, which is the field seen by the magnetic domains as explained in [2]:

$$\mathbf{h}_e = \mathbf{h} + \alpha_j \mathbf{m}. \tag{10}$$

The anhysteretic magnetization $\mathbf{m}_{an}$ is supposed in the same direction as the effective field $\mathbf{h}_e$, with magnitude m_{an}:

$$\mathbf{m}_{an} = m_{an}(h_e)\frac{\mathbf{h}_e}{h_e}, \tag{11}$$

where m_{an} is defined by the Langevin function:

$$m_{an}(h_e) = m_s\left[\coth\left(\frac{h_e}{a}\right) - \frac{a}{h_e}\right], \tag{12}$$

with notation $X = |\mathbf{X}|$ for the norm of a vector quantity $\mathbf{X}$. Note that equation (12) supposes that the considered material is isotropic. We obtain the differential anhysteretic susceptibility $d\mathbf{m}_{an}/d\mathbf{h}_e$:

$$\frac{d\mathbf{m}_{an}}{d\mathbf{h}_e} = \frac{1}{h_e}m_{an}(h_e)\left(\mathbf{1} - \frac{1}{{h_e}^2}\mathbf{h}_e\mathbf{h}_e\right) + \frac{dm_{an}(h_e)}{dh_e}\frac{1}{{h_e}^2}\mathbf{h}_e\mathbf{h}_e, \tag{13}$$

where $\mathbf{1}$ is the unit tensor and $\mathbf{h}_e\mathbf{h}_e$ the dyadic square of $\mathbf{h}_e$. According to [7], we consider a force $\boldsymbol{\chi}_f$' which impedes the wall displacements due to the pinning sites. This force is in the direction of $\mathbf{m}_{an} - \mathbf{m}_{irr}$:

$$\boldsymbol{\chi}_f' = \frac{1}{k}(\mathbf{m}_{an} - \mathbf{m}_{irr}). \tag{14}$$

According to [7], the irreversible magnetization changing $d\mathbf{m}_{irr}$ is considered in the direction of $\boldsymbol{\chi}_f$', so:

$$\frac{d\mathbf{m}_{irr}}{|d\mathbf{m}_{irr}|} = \frac{\boldsymbol{\chi}_f'}{|\boldsymbol{\chi}_f'|}. \tag{15}$$

The vector $d\mathbf{m}_{irr}$ is proportional to $\boldsymbol{\chi}_f' \cdot d\mathbf{h}_e$ and is zero when $\boldsymbol{\chi}_f' \cdot d\mathbf{h}_e$ is negative or null. So, $d\mathbf{m}_{irr}$ is written as follows:

$$d\mathbf{m}_{irr} = \frac{\boldsymbol{\chi}_f'}{|\boldsymbol{\chi}_f'|}(\boldsymbol{\chi}_f' \cdot d\mathbf{h}_e)^+, \tag{16}$$

with the notation of [7]: $(x)^+ = x$ if $x > 0$, $(x)^+ = 0$ if $x \leq 0$. We see that:

DOI:

$$\frac{\chi_f{}'}{|\chi_f{}'|} = \frac{\mathbf{m}_{an} - \mathbf{m}_{irr}}{|\mathbf{m}_{an} - \mathbf{m}_{irr}|} = \frac{\delta\mathbf{m}}{|\delta\mathbf{m}|}, \text{ where } \delta\mathbf{m} = \mathbf{m}_{an} - \mathbf{m}_{irr}. \tag{17}$$

In the case where $d\mathbf{h}_e \cdot \chi_f' > 0$, the change in irreversible magnetization is expressed as follows:

$$d\mathbf{m}_{irr} = \frac{1}{k}\frac{\delta\mathbf{m}}{|\delta\mathbf{m}|}(\delta\mathbf{m} \cdot d\mathbf{h}_e), \tag{18}$$

thus:

$$\frac{d\mathbf{m}_{irr}}{d\mathbf{h}_e} = \frac{1}{k}\frac{\delta\mathbf{m}\delta\mathbf{m}}{|\delta\mathbf{m}|}. \tag{19}$$

In the case where $d\mathbf{h}_e \cdot \chi_f' \leq 0$, the change in irreversible magnetization is considered to be zero:

$$\frac{d\mathbf{m}_{irr}}{d\mathbf{h}_e} = 0. \tag{20}$$

The equation which corresponds to the bulge of a wall for small displacement is:

$$\mathbf{m}_{rev} = c(\mathbf{m}_{an} - \mathbf{m}_{irr}). \tag{21}$$

By combining (9) and (21), the total magnetization is obtained:

$$\mathbf{m} = (1-c)\mathbf{m}_{irr} + c\mathbf{m}_{an}. \tag{22}$$

Irreversible magnetization is expressed in terms of the total magnetization and the anhysteretic magnetization:

$$\mathbf{m}_{irr} = \frac{\mathbf{m} - c\mathbf{m}_{an}}{1-c}. \tag{23}$$

We get:

$$\frac{d\mathbf{m}_{an}}{d\mathbf{m}} = \frac{d\mathbf{m}_{an}}{d\mathbf{m}_e}\frac{d\mathbf{m}_e}{d\mathbf{m}} = \frac{d\mathbf{m}_{an}}{d\mathbf{m}_e}\left(\mathbf{1} + \alpha_j \frac{d\mathbf{m}}{d\mathbf{h}}\right), \tag{24}$$

$$\frac{d\mathbf{m}_{irr}}{d\mathbf{m}} = \frac{d\mathbf{m}_{irr}}{d\mathbf{m}_e}\frac{d\mathbf{m}_e}{d\mathbf{m}} = \frac{d\mathbf{m}_{irr}}{d\mathbf{m}_e}\left(\mathbf{1} + \alpha_j \frac{d\mathbf{m}}{d\mathbf{h}}\right). \tag{25}$$

Finally, we obtain the following equation which governs the model:

$$\frac{\mathrm{d}\mathbf{m}}{\mathrm{d}\mathbf{h}} = \left[\mathbf{1} - \alpha_j \boldsymbol{\chi}\right]^{-1} \cdot \boldsymbol{\chi} \text{ with } \boldsymbol{\chi} = (1-c)\frac{\mathrm{d}\mathbf{m}_{\mathrm{irr}}}{\mathrm{d}\mathbf{h}_{\mathrm{e}}} + c\frac{\mathrm{d}\mathbf{m}_{\mathrm{an}}}{\mathrm{d}\mathbf{h}_{\mathrm{e}}}. \tag{26}$$

As $\mathbf{b} = \mu_0(\mathbf{h}+\mathbf{m})$, the differential permeability tensor is computed with:

$$\frac{\mathrm{d}\mathbf{b}}{\mathrm{d}\mathbf{h}} = \mu_0\left(\mathbf{1} + \frac{\mathrm{d}\mathbf{m}}{\mathrm{d}\mathbf{h}}\right). \tag{27}$$

The differential permeability tensor (27) is a 2×2 real matrix, which can easily be inverted. Doing so, we obtain the differential reluctivity tensor d**h**/d**b**:

$$\frac{\mathrm{d}\mathbf{h}}{\mathrm{d}\mathbf{b}} = \left(\frac{\mathrm{d}\mathbf{b}}{\mathrm{d}\mathbf{h}}\right)^{-1}. \tag{28}$$

We use the implicit Euler scheme to solve the time-domain finite element system of equations. Let Δt be the time step, t the previous instant and $t+\Delta t$ the current instant. We know the state at the previous instant ($\mathbf{h}_t$, $\mathbf{b}_t$) and the flux density at the current instant $\mathbf{b}_{t+\Delta t}$. The field $\mathbf{h}_{t+\Delta t}$ at the current instant, is then obtained with:

$$\mathbf{h}_{t+\Delta t} = \mathbf{h}_t + \int_t^{t+\Delta t}\left(\frac{d\mathbf{h}}{d\mathbf{b}}\frac{d\mathbf{b}}{dt'}\right)dt'. \tag{29}$$

Relation (29) is computed at the level of the material law, i.e. at each Gauss integration point during the integration and assembling of the FE system of equations (see subsection 2.4 below). The integral of (29) is computed by a time stepping procedure with a discretisation of 10 steps in the interval $[t,t+\Delta t]$.

The JA model presented in this subsection is already available in the GetDP software [26] and has been recently implemented in the Flux® software [27]. The implementations of the methods and simulations of the numerical examples that follow have been done with Flux® software.

As stated by [7], the equation (29) is implicit because the sign of $\mathrm{d}\mathbf{h}_e \cdot \boldsymbol{\chi}_f$' changes the expressions to compute **h**. To overcome this difficulty, we have chosen the following strategy. First we compute **h,** supposing $\mathrm{d}\mathbf{h}_e \cdot \boldsymbol{\chi}_f' > 0$. Then we compute the actual $\mathrm{d}\mathbf{h}_e \cdot \boldsymbol{\chi}_f$' and if it is negative, **h** is recomputed with $\mathrm{d}\mathbf{m}_{\mathrm{irr}}/\mathrm{d}\mathbf{h}_e = 0$.

The hysteresis model computes $\mathbf{h}_{t+\Delta t}$, with given $\mathbf{b}_{t+\Delta t}$, $\mathbf{b}_t$ and $\mathbf{h}_t$. For hysteresis models in general, the differential reluctivity and permeability tensors depend on the present state (**h**,**b**) of the material as well as on its "history". In the JA vector model presented in this subsection, the history is simply contained in the magnetic field at the previous instant $\mathbf{h}_t$. It is then necessary to store the magnetic field $\mathbf{h}_{t+\Delta t}$ computed by the model at the end of a time step, because it becomes the magnetic field $\mathbf{h}_t$ at the next step. We have chosen to store this quantity for each Gauss integration point used for the integrals of (6a).

As with JA hysteresis models in general, this vector hysteresis model does not lead to closed minor loops (centered or not centered), as reported e.g. by [7]. Some papers propose

DOI:

modifications of JA scalar models which represent accurately the minor loops, e.g. [16]. Unfortunately, to our knowledge, no paper proposes vector models with this improvement.

2.3. Low frequency lamination model

In the 2D finite element model, it is possible to take into account the eddy current losses in a laminated core of the magnetic circuit due to the in-plane flux density [3]. For the sake of simplicity, we assume a unitary stacking factor. We consider the case where the frequency is low, i.e. the skin effect is assumed to be negligible. So the flux density is approximately constant over the thickness of a lamination. From $\mathbf{curl}\,\mathbf{e} = -\mathrm{d}\mathbf{b}/\mathrm{dt}$, $\mathbf{j} = \sigma_{lam}\mathbf{e}$, $\mathbf{curl}\,\mathbf{h} = \mathbf{j}$, we can find the following expression:

$$\mathbf{h}_s(t) = \mathbf{h}_a(t) + \frac{\sigma_{lam} d^2}{12}\frac{d\mathbf{b}_a}{dt}, \tag{30}$$

where $\mathbf{h}_s$ is the magnetic field at the surface of a lamination, $\mathbf{h}_a$ and $\mathbf{b}_a$ the average magnetic field and flux density respectively, d the thickness of the lamination, and σ_{lam} their conductivity (assumed scalar and constant). The fields $\mathbf{h}_a$ and $\mathbf{b}_a$ are linked by the hysteresis model presented in subsection 2.2, with $\mathbf{h}_a = \mathbf{h}$ and $\mathbf{b}_a = \mathbf{b}$.

The total power density supplied to the lamination p(t) [W/m^3] reads:

$$p(t) = \mathbf{h}_s(t) \cdot \frac{d\mathbf{b}_a}{dt}. \tag{31}$$

The eddy current loss density $p_{cl}(t)$ [W/m^3], usually referred to as “classical losses”, corresponds to the second term of the right hand side (RHS) of (30):

$$p_{cl}(t) = \frac{\sigma_{lam} d^2}{12}\left(\frac{d\mathbf{b}_a}{dt}\right)^2. \tag{32}$$

And the power $p_h(t)$ [W/m^3], usually referred to as “hysteresis losses” corresponds to the first term of the RHS of (30):

$$p_h(t) = \mathbf{h}_a(t) \cdot \frac{d\mathbf{b}_a}{dt}. \tag{33}$$

In case of time-periodic supply of fundamental frequency f, to obtain total average loss density p_m (averaged over a time period), the total power density (31) is integrated over one fundamental period T = 1/f:

$$p_m = \frac{1}{T}\int_0^T \mathbf{h}_s(t) \cdot \frac{d\mathbf{b}_a}{dt}\,dt. \tag{34}$$

Applying the implicit Euler scheme, (30) becomes:

$$\mathbf{h}_{s\,t+\Delta t} = \mathbf{h}_{a\,t+\Delta t} + \frac{\sigma_{lam} d^2}{12\Delta t}\left(\mathbf{b}_{a\,t+\Delta t} - \mathbf{b}_{a\,t}\right), \tag{35}$$

with $\mathbf{h}_{a\,t+\Delta t}$ given by (29).

To introduce the lamination model in the FE model, the $\mathbf{h}(\mathbf{b})$ law is modified, from $\mathbf{h}_a(\mathbf{b}_a)$ given by (29) to $\mathbf{h}_s(\mathbf{b}_a)$ given by (35). The differential reluctivity tensor is modified as well from $d\mathbf{h}_a/d\mathbf{b}_a$ given by (28) to $d\mathbf{h}_s/d\mathbf{b}_a$:

$$\frac{d\mathbf{h}_s}{d\mathbf{b}_a} = \frac{d\mathbf{h}_a}{d\mathbf{b}_a} + \frac{\sigma_{lam} d^2}{12\Delta t}\mathbf{1}. \tag{36}$$

2.4. Newton-Raphson method and time stepping

The NR method is applied to solve the non-linear FE system [13] [14] with the implicit Euler scheme for time stepping. The extension to the generalized θ-method (with $0.5 \le \theta \le 1$) does not present any difficulty. The circuit equations are not considered here explicitly for sake of simplicity, but they are implemented in the software. The k-th NR iteration, k=1,2,…, produces the k-th approximation:

$$\mathbf{a}_{t+\Delta t}^{(k)} = \mathbf{a}_{t+\Delta t}^{(k-1)} + \alpha\, \Delta\mathbf{a}_{t+\Delta t}^{(k)}, \tag{37}$$

where the increment $\Delta\mathbf{a}_{t+\Delta t}^{(k)}$ follows from linearization of the system of equations (6b) around the (k-1)-th solution $\mathbf{a}_{t+\Delta t}^{(k-1)}$, with α the relaxation factor. The iterative scheme is initialized with $\mathbf{a}_{t+\Delta t}^{(0)} = \mathbf{a}_t$. To obtain the linearized system of equations, the residuals R_i given by (6a) are derived with respect to the nodal values a_j ($1 \le j \le n_p$):

$$\mathbf{J}\Delta\mathbf{a}_{t+\Delta t}^{(k)} = -\mathbf{R}, \tag{38}$$

with

$$\mathbf{J} = \left(\frac{d\mathbf{R}_{t+\Delta t}}{d\mathbf{a}}\right)_{\mathbf{a}_{t+\Delta t}^{(k-1)}} \quad \text{and} \quad \mathbf{R} = \mathbf{R}_{t+\Delta t}\left(\mathbf{a}_{t+\Delta t}^{(k-1)}\right),$$

where $\mathbf{a}$, $\Delta\mathbf{a}$ and $\mathbf{R}$ are the vector of the nodal values a_j, the vector of the increments Δa_j and the vector of the residuals R_i respectively. The Jacobian matrix $\mathbf{J}$ and RHS $-\mathbf{R}$ are function of the (k-1)-th solution $\mathbf{a}_{t+\Delta t}^{(k-1)}$. The (i,j) entry in the matrix $\mathbf{J}$ is [28]:

DOI:

$$J_{ij} = \int_{\Omega} \left(\mathbf{curl}\, \mathbf{W}_i \cdot \left(\frac{d\mathbf{h}}{da} \right)_{a_j{}^{(k-1)}_{t+\Delta t}} - \mathbf{W}_i \cdot \left(\frac{d\mathbf{j}}{da} \right)_{a_j{}^{(k-1)}_{t+\Delta t}} \right) d\Omega \,. \tag{39}$$

By using the chain rule and (1), (3), (4) and (5), the $\frac{d\mathbf{h}}{da_j}$ and $\frac{d\mathbf{j}}{da_j}$ terms are written:

$$\left(\frac{d\mathbf{h}}{da} \right)_{a^{(k-1)}_{j,t+\Delta t}} = \left(\frac{d\mathbf{h}}{d\mathbf{b}} \right)_{\mathbf{b}^{(k-1)}_{t+\Delta t}} \cdot \left(\frac{d\mathbf{b}^{(k-1)}_{t+\Delta t}}{da} \right)_{a^{(k-1)}_{j,t+\Delta t}} = \left(\frac{d\mathbf{h}}{d\mathbf{b}} \right)_{\mathbf{b}^{(k-1)}_{t+\Delta t}} \cdot \mathbf{curl}\, \mathbf{W}_j \tag{40}$$

$$\left(\frac{d\mathbf{j}}{da} \right)_{a^{(k-1)}_{j,t+\Delta t}} = \left(\frac{d\mathbf{j}}{d\mathbf{e}} \right)_{\mathbf{e}^{(k-1)}_{t+\Delta t}} \cdot \left(\frac{d\mathbf{e}^{(k-1)}_{t+\Delta t}}{da} \right)_{a^{(k-1)}_{j,t+\Delta t}} = -\sigma \left[\frac{d\left(\frac{\mathbf{a}^{(k-1)}_{t+\Delta t} - \mathbf{a}_t}{\Delta t} \right)}{da} \right]_{a^{(k-1)}_{j,t+\Delta t}} = -\frac{1}{\Delta t} \sigma \mathbf{W}_j \tag{41}$$

The final expression of the (i,j) entry of the Jacobian matrix **J** and RHS –**R** is thus:

$$J_{ij} = \int_{\Omega} \left(\mathbf{curl}\, \mathbf{W}_i \cdot \left(\frac{d\mathbf{h}}{d\mathbf{b}} \right)_{\mathbf{b}_{t+\Delta t}} \cdot \mathbf{curl}\, \mathbf{W}_j + \frac{1}{\Delta t} \mathbf{W}_i \cdot \sigma \cdot \mathbf{W}_j \right) d\Omega \,,$$

$$-R_i = \int_{\Omega} \left(\mathbf{W}_i \cdot \mathbf{j}_{t+\Delta t} - \mathbf{curl}\, \mathbf{W}_i \cdot \mathbf{h}_{t+\Delta t} \right) d\Omega \,. \tag{42}$$

In (42), if the lamination model is not used, $\mathbf{h}_{t+\Delta t}$ is given by (29) and $\left(d\mathbf{h}/d\mathbf{b}\right)_{\mathbf{b}_{t+\Delta t}}$ is given by (28). Otherwise, $\mathbf{h}_{t+\Delta t}$ is given by (35) and $\left(d\mathbf{h}/d\mathbf{b}\right)_{\mathbf{b}_{t+\Delta t}}$ by (36). The magnetic flux density is given by (1) and the current density $\mathbf{j}_{t+\Delta t}$ by (3) and (4c). The magnetic field $\mathbf{h}_{a,t+\Delta t}$ and the differential reluctivity tensor $\left(d\mathbf{h}_a/d\mathbf{b}_a\right)_{\mathbf{b}_{a,t+\Delta t}}$ are computed by the JA vector model presented in subsection 2.2. In (42), the magnetic field $\mathbf{h}_{a,t+\Delta t}$ is function of $\mathbf{b}^{(k-1)}_{a,t+\Delta t}$, $\mathbf{h}_{a,t}$ and $\mathbf{b}_{a,t}$, and the differential reluctivity tensor $\left(d\mathbf{h}_a/d\mathbf{b}_a\right)_{\mathbf{b}_{a,t+\Delta t}}$ is function of $\mathbf{h}^{(k-1)}_{a,t+\Delta t}$, $\mathbf{b}^{(k-1)}_{a,t+\Delta t}$, $\mathbf{h}_{a,t}$ and $\mathbf{b}_{a,t}$. It is necessary to store the magnetic field $\mathbf{h}^{(k)}_{a,t+\Delta t}$ computed by the JA model at the end of a k-th NR iteration, because it becomes the magnetic field $\mathbf{h}^{(k-1)}_{a,t+\Delta t}$ at the next NR iteration, which is necessary to compute $\left(d\mathbf{h}_a/d\mathbf{b}_a\right)_{\mathbf{b}_{a,t+\Delta t}}$. We store this magnetic field for each Gauss point.

2.5. Optimal relaxation coefficient method

In order to ensure the convergence of the NR method with the hysteresis model in most cases, a relaxation factor α is employed, which is calculated with the method described in [24]. This relaxation factor α is the same for all the unknowns and intervenes in (37). It is determined at the k-th NR iteration so as to minimize the square total residual $W^{(k)}$ of the linearized system of equations:

$$W^{(k)}(\alpha) = \sum_{i=1}^{n_p} \left(R_i^{(k)} \right)^2 . \tag{43}$$

We have to search for the optimal relaxation factor α_{opt} which minimizes $W^{(k)}$, with $0 < \alpha_{opt} \leq 1$. $W^{(k)}$ is function of α, as the $R_i^{(k)}$ are functions of α as well. A possibility is to use the binary search method, the golden section one or another minimum function searching method, but it would be too computationally expensive as mentioned in [24]. Finding an accurate value of α_{opt} is not needed, as the aim is to ensure the NR convergence and to reduce the whole CPU time of the simulation. So another strategy, proposed in [24], consists in trying consecutive integer powers of ½:

$$\alpha(m) = 1/2^m, \; (m = 0, 1, \ldots, m_{max}) . \tag{44}$$

Notice that the obtained value of α is not the optimal value α_{opt} (cf. figure 1). The objective function $W^{(k)}$ is computed with an iterative procedure starting with m = 0. At each iteration, the residuals must be computed, i.e. the RHS of the linearized system of equations must be integrated and assembled, which takes a certain CPU time. The process is stopped when the objective function starts to increase at the m-th current iteration, such as (cf. figure 1):

$$W^{(k)}(\alpha(m+1)) > W^{(k)}(\alpha(m)),$$

DOI:

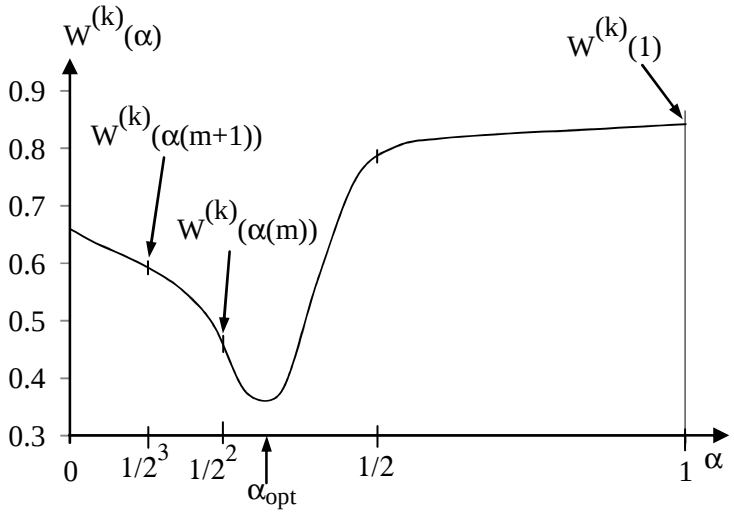

Figure 1. Example of a $W^{(k)}(\alpha)$ curve obtained at the 1st NR iteration of a test-case. The value of m found by the algorithm is m = 2, so $\alpha = 0.25$.

and the m-th relaxation coefficient is adopted for the current k-th NR iteration, i.e. $\alpha(m)=1/2^m$. We have tuned the maximum number of iterations m_{max} solving some numerical examples with the hysteresis model presented in subsection 2.2 and adopted $m_{max} = 12$. Numerical tests with an alternative minimum function searching method ("Residual Minimization" [29]) exhibited a lack of robustness in terms of convergence.

With the relaxation procedure (44) presented in this subsection, the NR algorithm has converged for every time step of all the numerical examples presented in this paper. This procedure is time consuming, because in some 2D practical cases with the JA hysteresis model, the computation time taken by this procedure can be 60 % of the total computation time of the solving process. However, without this procedure, the convergence is not achieved.

3. NUMERICAL EXAMPLES

3.1. Square region example

We have first tested the method on a simple case: a square domain (1 m side) with unidirectional pulsating or rotating field described in [14]. The JA model coefficients used for this study are those found in [14] and correspond to some electrical steel (FeSi): $m_s = 1.1455\times10^6$ A/m, a = 59 A/m, k = 99 A/m, c = 0.55 and $\alpha_j = 1.3\times10^{-4}$. We have verified that in the case of a pulsating field, the JA vector model gives the same results as the scalar one, according to the theory [7]. In the rotational case, the b and h loci are circular as expected.

We have also analyzed the number of time steps per period on the square domain test-case with pulsating imposed flux density, with two materials:

- 1st material: the electrical steel of [14], and
- 2nd material: car body steel with JA model coefficients $m_s = 1.5441\times10^6$ A/m, a = 672.919 A/m, k = 1138.68 A/m, c = 0.78054 and $\alpha_j = 1.0648\times10^{-3}$.

The mesh of the square domain consists of 1016 second order triangular elements. We performed simulations with 200, 300, 400, 800 and 1600 time steps per period of the imposed field. In the case of the first material, the convergence of the NR algorithm was achieved for all the time steps of all the simulations and the results were the same. In the case of the second material, we observed some convergence problems of the NR algorithm with the relaxation technique for the simulation with 200 time steps per period. With the other simulations, i.e. with a number of time steps per period greater or equal to 300, the convergence was reached for all the time steps and the results were the same.

3.2. T-joint and three-phase transformer

We have then performed simulations of two test cases concerning a three-phase transformer described in [3] operating at 50 Hz:

- a T-joint with imposed sinusoidal phase-shifted currents in two coils with $I_{max} = 0.01$A or $I_{max} = 0.2$A (cf. figure 2), and
- the whole three-phase transformer described in [3] operating at no load at 100 Vrms or 230 Vrms (cf. figure 3).

The coils have 220 turns in both test cases. The JA model coefficients used correspond to non-oriented M330-50A steel sheet [21]: $m_s = 1.28\times10^6$ A/m, $a = 26.1$ A/m, $k = 52.3$ A/m, $c = 0.13$ and $\alpha_j = 7.45\times10^{-5}$. A 1 s time interval, i.e. 50 periods, have been simulated, with 200 time steps per period by default. Simulations with 400 and 800 time steps per period produce the same results. So we concluded that 200 time steps per period were sufficient. The amplitude of the imposed currents or voltages are smoothly increased from 0 s until 0.8 s by a smoothed step function sf(t) so as to reduce the whole simulation time to reach the steady state and to converge at every time step ($sf(t) = 0.5 - 0.5\cos(\pi t/t_{relax})$ if $0 \leq t \leq t_{relax}$, $sf(t) = 1$ if $t > t_{relax}$, $t_{relax} = 0.8$ s). On the three-phase transformer, we have tried to impose the 100 V or 230 V voltage at the beginning of the simulation, without smoothly increasing it by a smoothed step function, with 200 time steps per period and without the lamination model. For the simulation at 100 V, the convergence is reached at all the time steps and we did not observe high inrush currents. For the simulation at 230 V, the algorithm diverges after 0.0038 s, probably due to high inrush currents. At the beginning of the simulation, i.e. at $t = 0$s, the magnetic field **h** and the flux density **b** are set to 0 in the whole regions where the hysteresis model is set, i.e. in the magnetic circuit. The simulation of several periods is necessary to obtain the periodic steady state. The curves depicted in the figures 4 and 5 of this subsection 3.2 are plotted for the 50th and last period, corresponding to time interval [0.98 s; 1 s].

DOI:

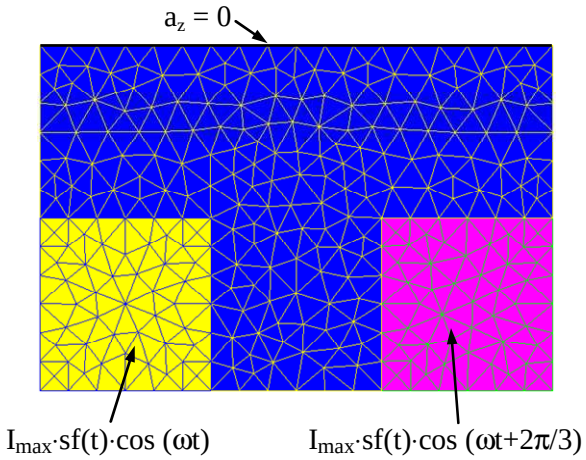

Figure 2. T-joint geometry and mesh.

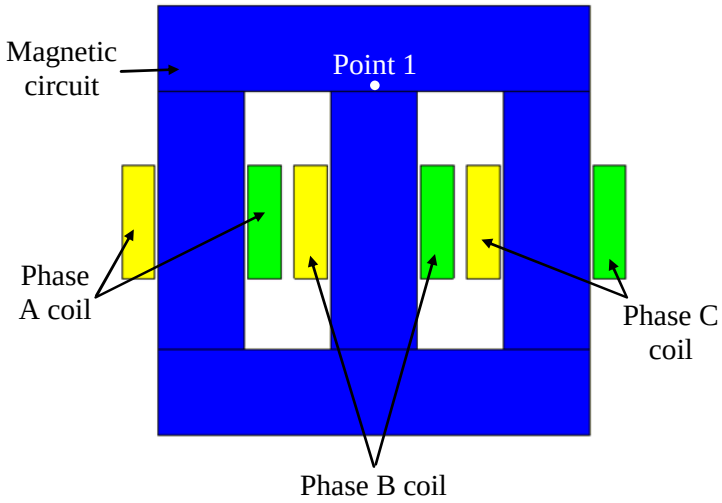

Figure 3. Three-limb transformer.

Both test cases have been simulated in two cases:

- Case 1: without the lamination model.
- Case 2: with the lamination model. A lamination is 0.5 mm thick and has a conductivity of 2.03×10^6 S/m.

With the T-joint test case, we have also taken into account eddy currents in the z-direction by considering that the magnetic circuit is solid, i.e. not laminated, with a 500 S/m conductivity and a zero net current (referred to as case 3 in the following).

In average 7 and 8 NR iterations are performed per time step for the transformer at 100 Vrms and 230 Vrms respectively.

With a current of 0.01A (peak value) in the coils of the T-joint and with the transformer at 100 V, a drift of flux density and also a drift of magnetic field, however to a lesser extent, are observed after 0.7 s in cases 1 and 2. It is much reduced in case 3 (with massive magnetic circuit) of the T-joint, but with also very different results. With a current of 0.2 A in the coils of the T-joint and with the transformer at 230 V, the simulation results do not exhibit any drift of flux density in time. An explanation may be that, in these cases, most of the points of the magnetic circuit are saturated and this contributes to stabilize the model.

Figure 4 shows the $b_{ax}h_{sx}$- and $b_{ay}h_{sy}$-loops obtained at point 1. The appearance is almost the same as the loops of figure 14 of [3]. However, the materials of laminations are not exactly the same: M330-50A for present paper and V330-50A in [3].

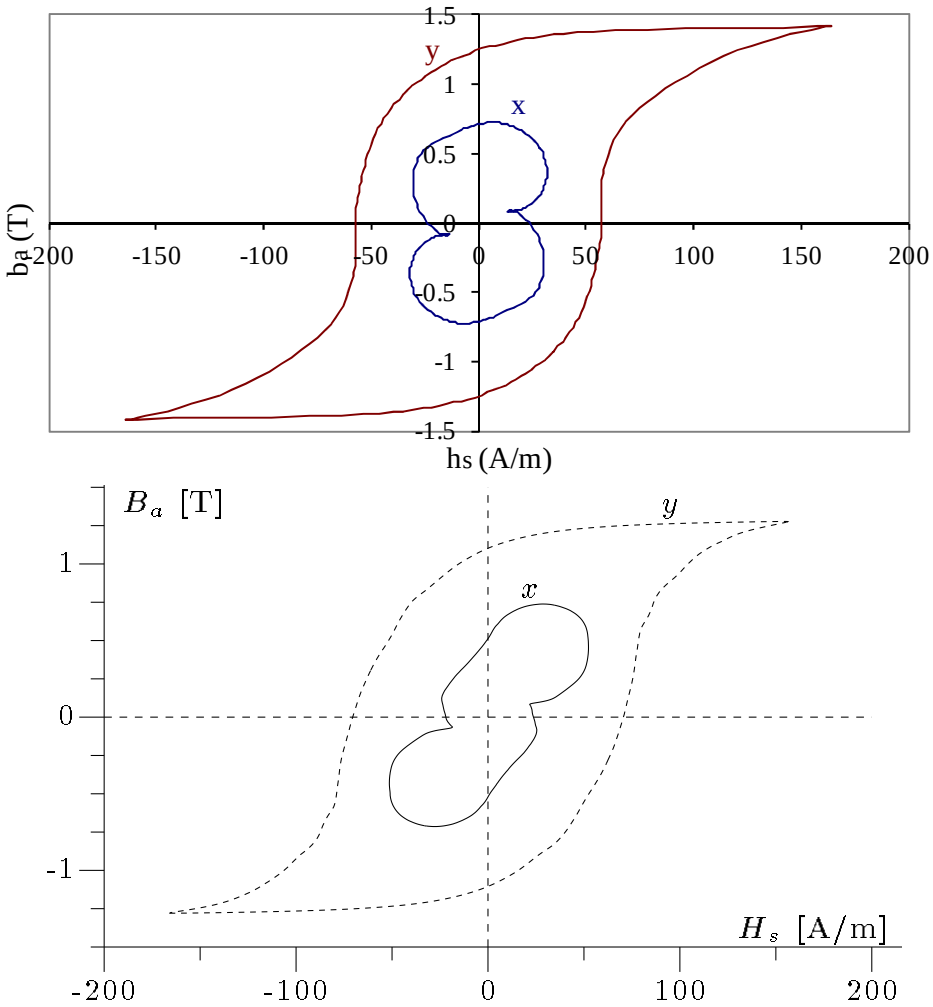

Figure 4. $b_{ax}h_{sx}$- and $b_{ay}h_{sy}$-loops at point 1 of the transformer for a voltage of 230 V with the lamination model. Top: with the approach of the present paper. Bottom: figure 14 of [3].

Figure 5 shows currents in the three phases as a function of time at the last period of simulation, with and without the lamination model. The amplitude of the current is slightly greater with the lamination model than without, as expected, because of the greater loss and supplied power in the case of the lamination model.

DOI:

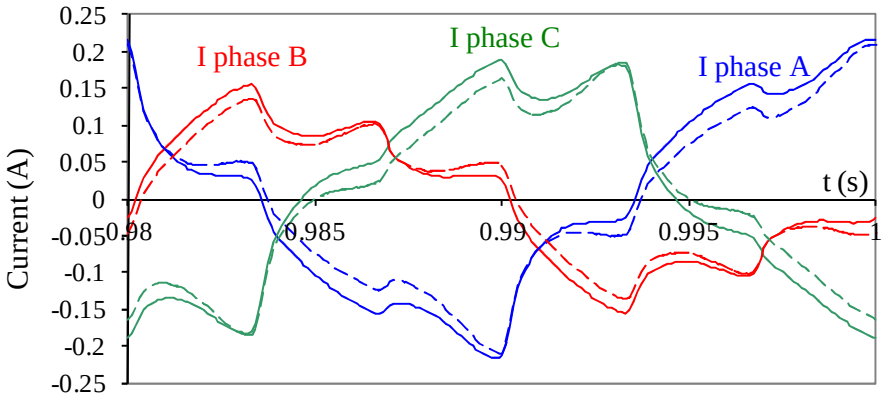

Figure 5. Transformer phase currents for a voltage of 230 V. Dashed line: without the lamination model, continuous line: with the lamination model.

3.3. TEAM workshop problem 32

We have also performed a 2D simulation of the TEAM workshop problem 32 described in [30]. The device consists of a single-phase 3-limb transformer with the windings placed on the outer limbs (cf. figure 6). The ferromagnetic core consists of five 0.48 mm thick non-oriented laminations. This workshop problem comprises four different cases. As in [12], we have simulated the CASE3 (so denoted in [30]). The two windings are fed by 14.5 V (peak) voltage sources with a phase shift of 90° at a frequency of 10 Hz (cf. figure 7). So the magnetic field and flux density are rotating in the T-joints. A vector hysteresis model is therefore necessary.

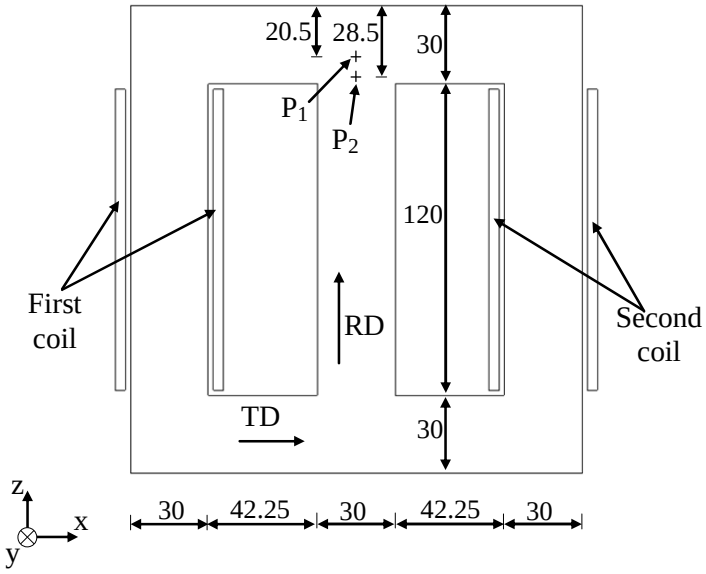

Figure 6. Problem 32 transformer: geometry with dimensions (in mm) and positions of the pick-up coils. Pick-up coils C1-C2 and C3-C4 described in [30] correspond to points P_1 and P_2 respectively.

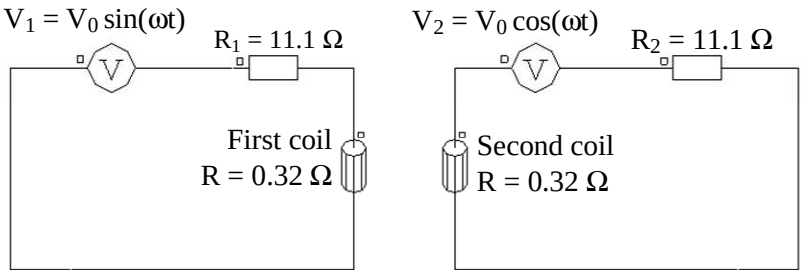

Figure 7. External circuit (V_0 = 14.5V, f = 10 Hz).

In [30], the data of the ferromagnetic material measurements, i.e. h and b for several centered loops, are provided in all directions. A different magnetic behavior in the vertical (rolling direction, RD) and in the horizontal direction (transverse direction, TD) is observed. Using an optimizing procedure, the authors of [12] have found the JA model coefficients in the RD and in the TD from the data of the ferromagnetic material measurements provided in [30]. However, as the hysteresis model described in the present paper is only valid for isotropic magnetic materials, we have adopted the same hysteresis data in both directions. We took the JA coefficients corresponding to the RD found in [12], i.e. $m_s = 1.33\times10^6$ A/m, a = 172.856 A/m, k = 232.652 A/m, c = 0.652 and $\alpha_j = 417\times10^{-6}$. As the frequency is low, the lamination model has not been used. The relaxation procedure is necessary for the simulation. With it, the NR algorithm converges for all the time steps. Without it, the convergence is not reached at the first time step. In average 5 NR iterations are performed per time step on this numerical example. We have simulated 4 periods with 200 time steps per period. The steady state is reached at the second period. The simulation lasted one hour and 23 minutes on a PC with Intel® i7-3740QM at 2.7 GHz CPU with 8 cores.

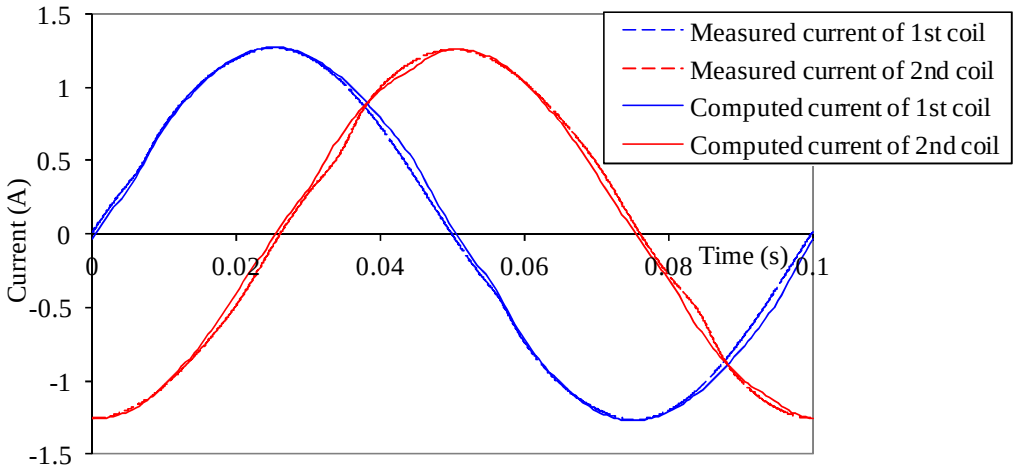

Figure 8. Currents in the two coils versus time.

Figure 8 shows the measured and computed currents in the two coils. Results exhibit an excellent agreement. We notice that the currents are almost sinusoidal functions of time. The RMS value error on the current is 3.9 % and 4.9 % in the first coil and in the second coil respectively.

DOI:

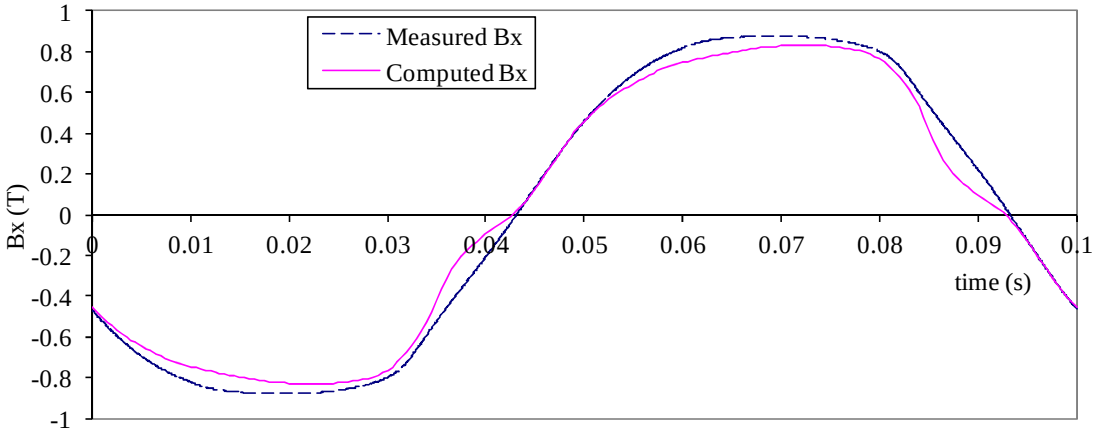

Figure 9. x-components of b function of time at point P_1 (pick-up coils C1-C2).

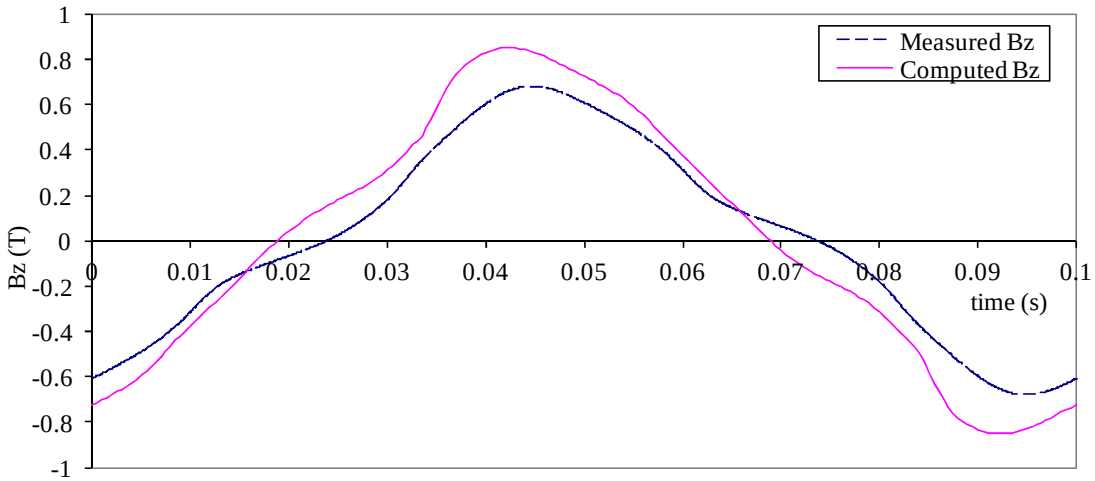

Figure 10. z-components of b versus time at point P_1 (pick-up coils C1-C2).

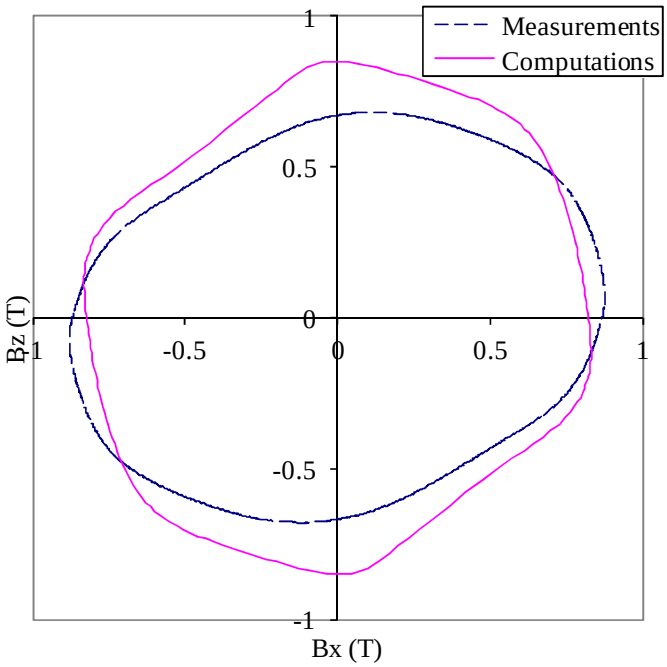

Figure 11. $b_x b_z$-locus at point P_1 (pick-up coils C1-C2).

In figures 9-11 and 12-14, the flux density at points 1 and 2 respectively is depicted. The measured and computed curves have the same shapes and a small difference between computed results and measurements is observed. This validates our model and our approach, though it is valid for isotropic materials only. The authors of [12] used an anisotropic hysteresis model, which explains the smaller error there.

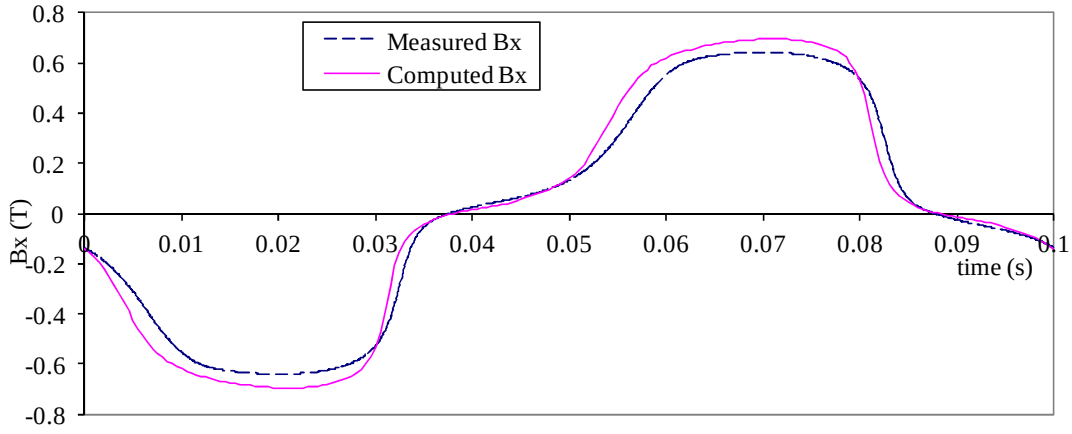

Figure 12. x-component of b versus time at point P_2 (pick up coils C3-C4).

DOI:

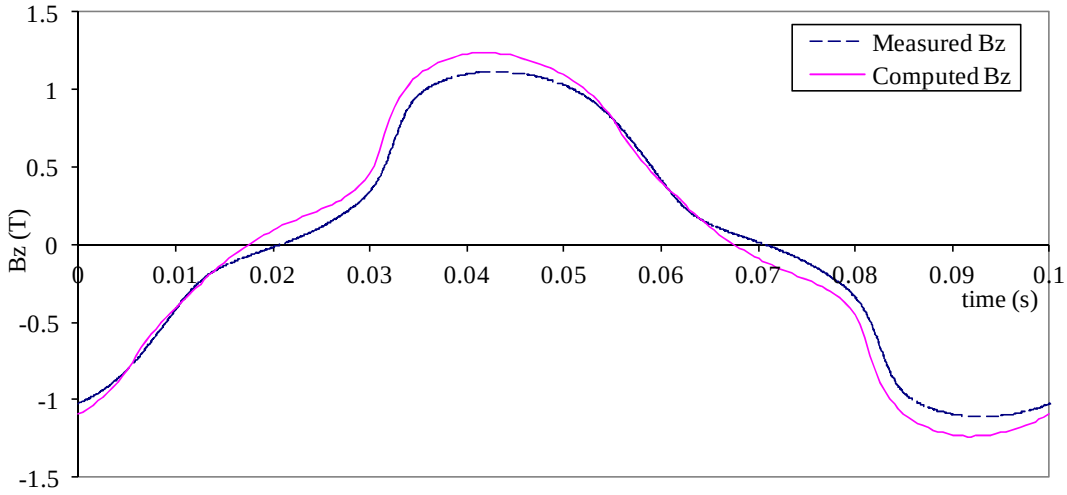

Figure 13. z-components of b versus time at point P_2 (pick up coils C3-C4).

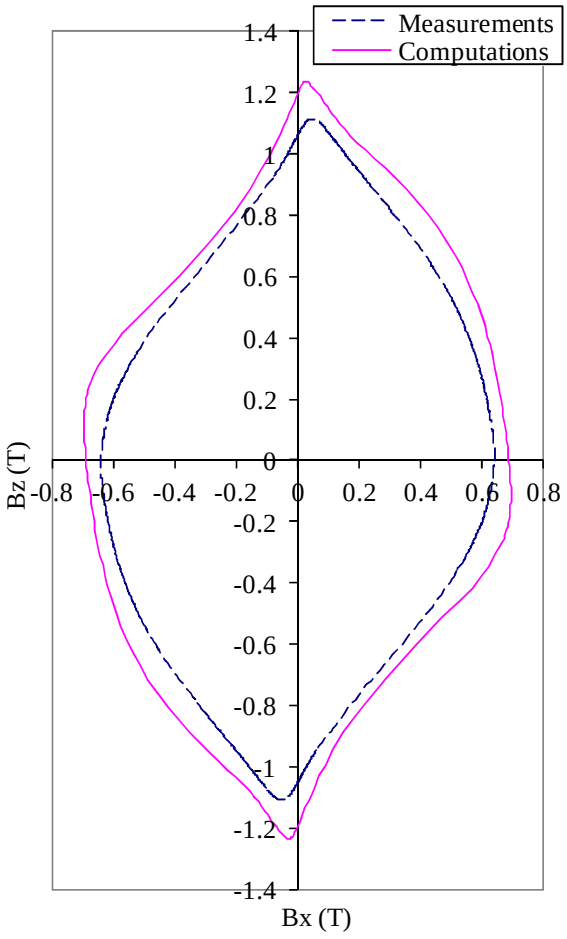

Figure 14. $b_x b_z$-locus at point P_2 (pick up coils C3-C4).

5. CONCLUSIONS

We have simulated a square domain test case and two 2D transformer models using an inverse JA vector model for isotropic magnetic materials. On the square domain test case, we

have analyzed the number of time steps per period. A number of 200 time steps per period has been determined as the minimum to reach the convergence with the relaxation procedure used with the NR algorithm. Good convergence has been observed with the other test cases with the proposed approach. We have simulated a three-phase transformer on which we computed the currents in the three phases and the b(h) loop at a point in the T-joint area, where the fields are rotating. At reduced voltage, an unstable behavior has been observed with the hysteresis model: a drift of the flux density function of time is observed. This drift is not present at rated voltage, where almost the whole magnetic circuit is saturated, which contributes to stabilize the model. We have validated the model on another numerical example, the TEAM workshop problem 32. We computed the currents in the coils and the magnetic flux density function of time at two points in the T-joint area. On this numerical example, we obtained a good agreement between computed and measured results. We think that the JA vector model is well adapted to the simulation of electrical devices such as transformers or electromechanical actuators, with a supply of only one frequency, i.e. without harmonics, as this model does not lead to closed minor loops. We think that this JA model is well adapted to simulate the transient operation of fast-acting electromechanical actuators, accounting for remanence in the ferromagnetic parts, which will be the subject of a further paper. In a future work, instability problems of the hysteresis model with reduced currents and voltages must be overcome. Extensions to 3D analysis and anisotropic materials are also envisaged.

REFERENCES

1. I. D. Mayergoyz, *Mathematical models of hysteresis and their applications*, Elsvier: New-York, 2003.
2. D. Jiles, P. Atherton, Theory of ferromagnetic hysteresis, *Journal of Magnetism and Magnetic Materials*, 61, issue 1-2, 48–60, 1986.
3. J. Gyselinck, M. De Wulf, L. Vandevelde, and J. Melkebeek, Incorporation of vector hysteresis and eddy current losses in 2D FE magnetodynamics, in Proc. Electrimacs'99, Lisbon, Portugal, Sept., 14–16, 1999 ; **3**, 37–44.
4. I.D. Mayergoyz, Mathematical models of hysteresis, *IEEE Transactions on Magnetism* 1986; **22(5)** : 603–608.
5. E. Dlala, Efficient Algorithms for the inclusion of the preisach hysteresis model in nonlinear finite-element methods, *IEEE Transactions on Magnetism* 2011; **47(2)** : 395–408.
6. N. Sadowski, N.J. Batistela, J.P.A. Bastos and M. Lajoie-Mazenc, An inverse Jiles-Atherton model to take into account hysteresis in time-stepping finite-element calculations, *IEEE Transactions on Magnetism* 2002; **32(5)** : 797–800.
7. A. Bergqvist, A simple vector generalisation of the Jiles–Atherton model of hysteresis, *IEEE Transactions on Magnetism*1996; **32(5)** : 4213–4215.
8. J.V. Leite, N. Sadowski, P. Kuo-Peng, N. J. Batistela, J.P.A. Bastos and A.A. de Espíndola, Inverse Jiles-Atherton vector hysteresis model, *IEEE Transactions on Magnetism* 2004; **40(4)** : 1769–1775.
9. J. V. Leite, A. Benabou and N. Sadowski, Transformer inrush currents taking into account vector hysteresis, *IEEE Transactions on Magnetism* 2010; **46(8)** : 3237–3240.
10. J.V. Leite, A. Benabou, N. Sadowski, S. Clenet, J.P.A. Bastos and F. Piriou, Implementation of an anisotropic vector hysteresis model, *IEEE Transactions on Magnetism* 2008; **44(6)** : 918–921.
11. K. Hoffmann, J.P.A. Bastos, N. Sadowski and J. V. Leite, Convergence Procedures Applied for Solving 3D Vector Hysteresis Modeling Coupled with FEM, *CEFC'2014*, Annecy, France, 2014.
12. J.P.A. Bastos, N. Sadowski, J.V. Leite, N.J. Batistela, K. Hoffmann, G. Meunier, and O. Chadebec, A differential permeability 3-D formulation for anisotropic vector hysteresis analysis, *IEEE Transactions on Magnetism* 2014; **50(2)**, DOI: 10.1109/TMAG.2013.2282697.

13. J. Gyselinck, L. Vandevelde, J. Melkebeek and P. Dular Complementary two-dimensional finite element formulations with inclusion of a vectorized Jiles-Atherton model, *COMPEL* 2004; **23(4)** : 959–967.

14. J. Gyselinck, P. Dular, N. Sadowski, J. Leite and J.P.A. Bastos, Incorporation of a Jiles-Atherton vector hysteresis model in 2D FE magnetic field computations – Application of the Newton-Raphson method, *COMPEL* 2004; **23(3)** : 685–693.

15. M. Chiampi, D. Chiarabaglio and M. Repetto, A Jiles-Atherton and fixed-point combined technique for time periodic magnetic field problems with hysteresis, *IEEE Transactions on Magnetism* 1995; **31(6)** : 4306–4311.

16. J.V. Leite, N. Sadowski, P. Kuo-Peng and A. Benabou, Minor loops calculation with a modified Jiles-Atherton hysteresis model, *Journal of Microwaves, Optoelectronics and Electromagnetic Applications* June 2009; **8(1)** : 49–55.

17. A. Nourdine, G. Meunier and A. Kedous-Lebouc, Numerical computation of a vectorial hysteresis H(B) magnetization law, *IEEE Transactions on Magnetism* 2014; **50(2)** : 1393– 1396.

18. K. Jacques, R. V. Sabariego, C. Geuzaine, and J. Gyselinck, Inclusion of a direct and inverse energy-consistent hysteresis model in dual magnetostatic finite element formulations, *IEEE Transactions on Magnetism* 2015; DOI: 10.1109/TMAG.2015.2490578.

19. A. Bergqvist, Magnetic vector hysteresis model with dry friction-like pinning, *Physica B* 1997; **233(4)** : 342–347.

20. D. Lin, P. Zhou, and A. Bergqvist, Improved vector play model and parameter identification for magnetic hysteresis materials, *IEEE Transactions on Magnetism* 2003; **39(3)**, DOI: 10.1109/TMAG.2013.2281567.

21. K. Chwastek, The applications of fixed-point theorem in optimisation problems, *Archives of Electrical Engineering* 2012; **61(2)** : 189–198.

22. M.A. Zaman and M.A. Matin, Optimization of Jiles-Atherton hysteresis model parameters using Taguchi's method, *IEEE Transactions on Magnetism* 2015; **51(5)**.

23. M.A. Zaman and U. Sikder, Bouc–Wen hysteresis model identification using Modified Firefly Algorithm, *Journal of Magnetism and Magnetic Materials*, 2015; **395** : 229–233.

24. K. Fujiwara, T. Nakata, N. Okamoto, and K. Muramatsu, Method for determining relaxation factor for modified Newton-Raphson method, *IEEE Transactions on Magnetism* 1993; **29(2)** : 1962–1965.

25. G. Meunier, *The finite element method for electromagnetic modeling*, ISTE, Wiley, Chapter 7, *Coupling with circuit equations*, 277–320, 2008.

26. P. Dular, C. Geuzaine, F. Henrotte and W. Legros, A general environment for the treatment of discrete problems and its application to the finite element method, *IEEE Transactions on Magnetism*1998; **34(5)** : 3395–3398.

27. Flux software, www.cedrat.com.

28. G. Meunier, *The finite element method for electromagnetic modeling*, chapter 5, Behaviour laws of materials, ISTE: London, 2008.

29. K. Fujiwara, Y. Okamoto, A. Kameari and A. Ahagon, The Newton–Raphson method accelerated by using a line search—comparison between energy functional and residual minimization, *IEEE Transactions on Magnetism* 2005; **41(5)** : 1724–1727.

30. O. Bottauscio, M. Chiampi, C. Ragusa, L. Rege and M. Repetto, Description of TEAM problem: 32 A – test case for validation of magnetic field analysis with vector hysteresis, 2010, [online] Available: http://www.compumag.org/jsite/images/stories/TEAM/problem32.pdf and http://www.cadema.polito.it/team32